Bioorganic & Medicinal Chemistry Letters 23 (2013) 3741–3748

Contents lists available at SciVerse ScienceDirect

Bioorganic & Medicinal Chemistry Letters

journal homepage: www.elsevier.com/locate/bmcl

Discovery of NVP-BYL719 a potent and selective phosphatidylinositol-3 kinase alpha inhibitor selected for clinical evaluation

Pascal Furet, Vito Guagnano, Robin A. Fairhurst, Patricia Imbach-Weese, Ian Bruce, Mark Knapp, Christine Fritsch, Francesca Blasco, Joachim Blanz, Reiner Aichholz, Jacques Hamon, Doriano Fabbro, Giorgio Caravatti *

Novartis Institutes for BioMedical Research, WKL-136.4.12, CH-4002 Basel, Switzerland

ARTICLE INFO

Article history:
Received 25 March 2013
Revised 30 April 2013
Accepted 4 May 2013
Available online 14 May 2013

Keywords:
PI3K inhibitors
Antitumor agent

ABSTRACT

Phosphatidylinositol-3-kinase α (PI3Kα) is a therapeutic target of high interest in anticancer drug research. On the basis of a binding model rationalizing the high selectivity and potency of a particular series of 2-aminothiazole compounds in inhibiting PI3Kα, a medicinal chemistry program has led to the discovery of the clinical candidate NVP-BYL719.

© 2013 Elsevier Ltd. All rights reserved.

Phosphatidylinositol-3-kinases (PI3Ks) are lipid kinases that are important in controlling signaling pathways involved in cell proliferation, motility, cell death and cell invasion.[1,2] Human cells contain three genes (*PIK3CA*, *PIK3CB* and *PIK3CD*) encoding the catalytic subunits of class IA PI3K enzymes, termed p110α, p110β and p110δ. P110α and p110β are expressed in most tissues, whereas p110δ is expressed primarily in leukocytes. The class IB PI3K consists of only one enzyme, PI3Kγ. Its catalytic subunit, p110γ, is encoded by *PIK3CG* and is also expressed primarily in leukocytes.

Dysregulation of the PI3K signaling pathway is implicated in many human cancers[3,4] and includes the inactivation of the PTEN tumor suppressor gene,[5] amplification/overexpression or activating mutations of some receptor tyrosine kinases (e.g., erbB3, erbB2, EGFR), and amplification of genomic regions containing *AKT* or *PIK3CA* genes.[6–8] In addition, it was found that *PIK3CA* is somatically mutated in many human cancers, for example, in 32% of colorectal cancers,[9] 27% of glioblastomas,[9,10] 25% of gastric cancers,[9–11] 36% of hepatocellular carcinomas,[12] and 18–40% of breast cancers.[13–16] From these mutation frequencies, *PIK3CA* is one of the two most commonly mutated genes identified in human cancers. No mutations of *PIK3CB*, *PIK3CD*, and *PIK3CG* have been identified.

As most p110α mutations constitutively activate its kinase activity, PI3Kα appears to be an ideal target for drug development. Indeed, several low molecular weight compounds are under active clinical development, including pan-PI3K inhibitors such as GDC-0941,[17] XL-147,[18] BKM120,[19] ZSTK-474,[20] and CH-5132799[21] and p110α isoform-specific inhibitors such as INK-1117.[18] P110α isoform-specific inhibitors may exhibit anti-cancer activity in PI3Kα mutant tumors without causing the potential side effects that could be expected from interference with the other isoforms.

Here we report about the medicinal chemistry aspects of the discovery of NVP-BYL719, an α-specific PI3K inhibitor from the 2-aminothiazole class which entered clinical trials in 2010.

It has previously been reported that the 2-aminothiazole scaffold is a valuable template to obtain PI3K inhibitors showing isoform selectivity.[22] In particular, it was found that attaching a (*S*)-pyrrolidine carboxamide moiety to the 2-amino group through an urea linkage confers selectivity for the α isoform in this class of PI3K inhibitors as exemplified by compound **1** (Fig. 1).[22] We were interested to optimize this type of selective PI3Kα inhibitors towards compounds suitable for pharmacological studies in animal tumor models. Among the different potent analogs of **1** available at the onset of the program, compound **2** (Table 1) was selected as the starting point of this effort. To guide the optimization process, we decided to construct a binding model of **2** in the ATP pocket of the kinase domain of PI3Kα. To this end we used the crystal structure of the human p110α/p85α complex reported by Huang et al.,[23] the only PI3Kα structure that was available at the time we initiated the work reported in this Letter. We docked[24] **2** in the unliganded ATP pocket of the kinase domain

* Corresponding author. Tel.: +41 61 696 5844; fax: +41 61 696 2455.
E-mail address: giorgio.caravatti@novartis.com (G. Caravatti).

0960-894X/$ - see front matter © 2013 Elsevier Ltd. All rights reserved.
http://dx.doi.org/10.1016/j.bmcl.2013.05.007

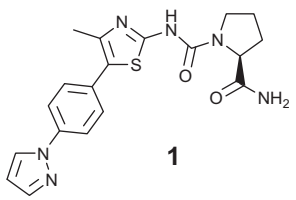

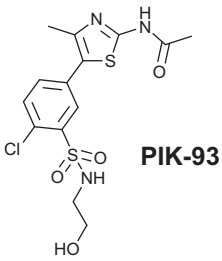

Figure 1. Chemical structures of PI3Kα selective 2-aminothiazole derivative **1**[22] and PIK-93.

of this structure with the same binding mode as that of a related unselective 2-aminothiazole PI3K inhibitor, PIK-93, observed in a co-crystal structure with PI3Kγ.[25] This implied an orientation in which the thiazole nitrogen and the 2-NH group of **2** form bidentate hydrogen bonds with the backbone NH and carbonyl of PI3Kα residue V851 while its pyrimidine moiety sits in the less solvent accessible part of the cavity, the so called affinity pocket, formed by residues Y836, I932, I848, I800, D933, K802, P778 and M772. Placing the inhibitor in the cavity in such a way immediately provided a hypothesis for the structural basis of the α isoform selectivity of the 2-aminothiazole inhibitors carrying the (*S*)-pyrrolidine carboxamide urea moiety. As shown in Figure 2 this binding mode allows the amide group of the latter to form three hydrogen bonds with PI3Kα, exploiting the full potential of a primary amide group for such interactions. In one of them the inhibitor amide nitrogen is a donor for the backbone carbonyl of residue S854 while the two others involve both the amide carbonyl and nitrogen that engage in donor–acceptor interactions

Table 1
Inhibition of p110α, p110β, p110δ and p110γ activity (biochemical assay), in vitro metabolic clearance using rat liver microsomes and CYP450 3A4 inhibition

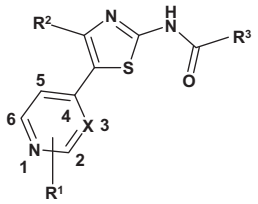

Compound	R^1	X	R^2	R^3	IC_{50}[a] (μM)				Microsomal CL, rat (μL min^{-1} mg^{-1})	CYP450 3A4 IC_{50} (μM)
					P110α	P110β	P110δ	P110γ		
2	2-*tert*-Bu	N	CH_3	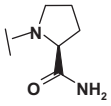	0.0075	1.8	0.35	0.21	62[b]	>10
3	2-*tert*-Bu	CH	CH_3	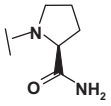	0.014	4.4	0.33	0.43	77[b]	>10
4	2-*tert*-Bu	CH	CH_3	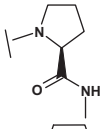	2.7	>9.1	4.2	4.6	104[b]	n.d.
5	2-*tert*-Bu	CH	CH_3	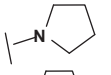	0.62	4.9	0.59	0.93	186[b]	n.d.
6	2-*tert*-Bu	CH	CH_3	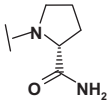	>9.1	8.2	3.3	>10	36[b]	n.d.
7	2-*tert*-Bu	N	CH_3	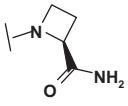	0.019	1.2	0.29	0.32	44	n.d.
8		CH	CH_3	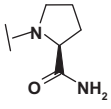	0.005	1.2	0.29	0.25	29	>10
9	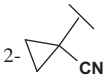	CH	CH_3	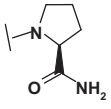	0.019	4.1	2.0	1.1	41	>10
10	2-*iso*-Pr	N	CH_3	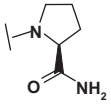	0.016	4.0	0.96	1.4	36	>10

Table 1 (*continued*)

Compound	R^1	X	R^2	R^3	IC_{50}[a] (μM)				Microsomal CL, rat (μL min^{-1} mg^{-1})	CYP450 3A4 IC_{50} (μM)
					P110α	P110β	P110δ	P110γ		
11	2-*cyclo*-Bu	N	CH_3	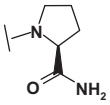	0.020	1.8	0.69	0.61	53	>10
12	6-*iso*-Pr	N	CH_3	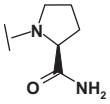	0.32	>9.1	n.d.	n.d.	n.d.	n.d.
21		CH	H	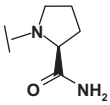	0.0095	3.9	1.1	0.83	27	>10
22		CH	Cl	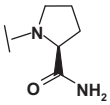	0.039	5.5	0.43	1.4	17	n.d.
27	2-Diethylamino	N	CH_3	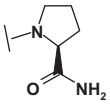	0.016	1.2	0.34	0.41	96	n.d.
28		N	CH_3	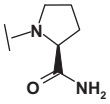	0.012	3.1	0.81	0.69	47	>10

[a] The values are averages of at least two separate determinations.[27]
[b] Includes the cofactor for glucuronyl transferases UDPGA.

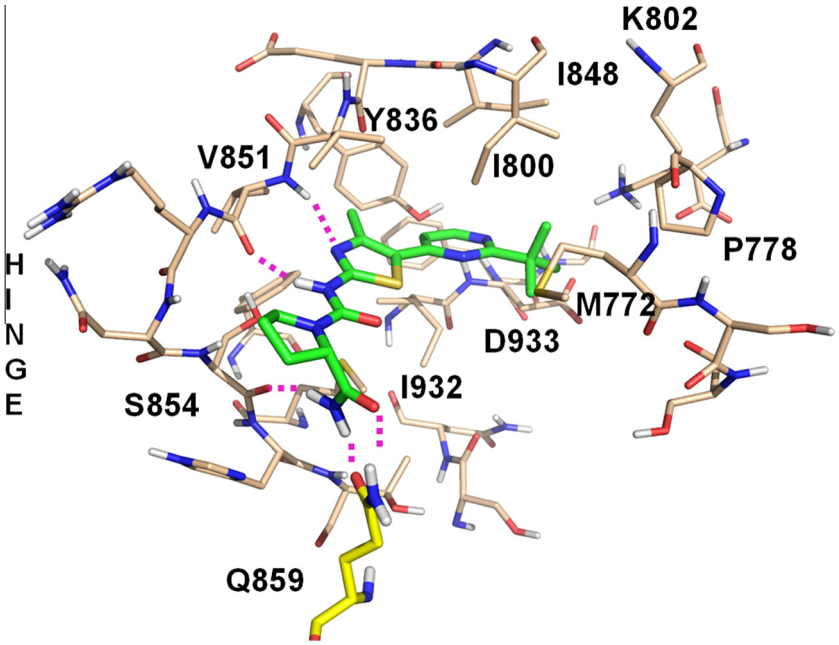

Figure 2. Proposed binding mode of compound **2** in the ATP pocket of PI3Kα. Hydrogen bonds are represented as dashed lines.

with the side chain amide group of residue Q859. The former hydrogen bond, being made with the backbone of the protein, can also exist in the other PI3K isoforms. In contrast, residue Q859 is not conserved within the PI3K family. Isoforms β, δ and γ have an aspartic acid, an asparagine and a lysine residue, respectively, at this position. The aspartic acid and lysine residues of the β and γ isoforms are obviously not able to establish the same hydrogen bond donor–acceptor interactions with the primary amide group of the inhibitor as a glutamine. In principle, the side chain of the δ isoform asparagine could form such interactions. However, a simple modeling experiment in which Q859 was mutated into an asparagine indicated that the shorter side chain of this amino acid did not allow the donor–acceptor hydrogen bonds to be formed without compromising the other favorable interactions of the inhibitor with the ATP pocket. The docking model thus strongly suggested that the PI3Kα selectivity

of **2** and its analogs originated in the formation of two stabilizing specific hydrogen bonds with the side chain of Q859, interactions that are not possible with the other isoforms.

The model was used to design modifications of **2** aimed at modulating the compound physico-chemical properties while preserving its high potency. For instance, following the observation that in the model, the pyrimidine N3 nitrogen of the inhibitor did not make any polar interaction with the ATP pocket, we expected no significant loss of activity by replacing it by a carbon atom. Indeed, the resulting pyridine analog **3** turned out to be as potent in inhibiting PI3Kα as **2** with the same selectivity profile.[26] Analogues of **3** with alterations in the pyrrolidine carboxamide moiety were then envisaged to probe our PI3Kα selectivity concept. Methylation of the amide group (compound **4**), its removal (compound **5**) or inversion of the stereochemistry (compound **6**) resulted in unselective micromolar inhibitors, a consequence of dramatic losses of PI3Kα inhibitory activity. These results gave strong support to the postulated bidentate hydrogen bonds with Q859 as the structural determinant of PI3Kα selectivity in this class of inhibitors. Interestingly, replacement of the prolineamide moiety in **2** by the corresponding azetidine derivative led to a slight decrease of PI3Kα inhibition while the level of PI3Kβ, PI3Kδ and PI3Kγ inhibition was maintained (compound **7**). According to the binding model, this effect could be ascribed to a loss of one favorable van der Waals contact with the imidazole ring of the side chain of PI3Kα residue H855 caused by reducing the ring size to four atoms. In contrast, PI3Kβ, PI3Kδ and PI3Kγ, having respectively, a glutamic acid, an aspartic acid and a threonine residue at the corresponding position in their sequence, cannot form such an interaction with the prolineamide moiety.

Another example of modification inspired by the binding model was the replacement of one of the methyls of the *tert*-butyl group of **2** or **3** by a trifluoromethyl or a cyano substituent. As shown in Figure 3, the model suggested that the *tert*-butyl group did not fully occupy the space available in a small cavity formed by the side chains of residues I800, I848, P778 and K802. In the direction of one of the methyls there was some space left allowing the accommodation of a slightly larger group, such as a trifluoromethyl one, in the small cavity. Another of the *tert*-butyl methyls was pointing towards the amino group of the side chain of K802. This led to the idea of replacing it by a cyano group targeting K802 for hydrogen bonding. Consistent with these notions, the resulting analogs of **3**, **8** and **9**, showed potent and selective inhibition of PI3Kα while the analogs of **2** having smaller substituents such as the *iso*-propyl or *cyclo*-butyl group (compounds **10** and **11**, respectively) at this position were slightly less active than the latter in inhibiting PI3Kα. Replacement of the *tert*-butyl group in **2** by the slightly larger diethylamino group (compound **27**) did not lead to an improvement in activity likely due to the different shape of this substituent.[28]

The model could also explain the significant loss of activity observed with the 6-*iso*-propyl pyrimidine isomer (compound **12**) of **10**. Assuming the same binding mode for this compound orients its pyrimidine N3 nitrogen towards the hydrophobic wall of the cavity in the region corresponding to the side chain of Y836 where it is unable to form a hydrogen bond compensating for the solvation energy lost upon binding.

The synthetic routes to prepare the 2-aminothiazole derivatives are outlined in Schemes 1 and 2. In the synthesis of the 5-(4-pyridinyl) substituted derivatives the key step was the palladium-catalyzed direct arylation of 4-methyl-2-acetaminothiazole with a 4-bromopyridine following a method developed in the group of Miura.[29] This is exemplified in Scheme 1 for the synthesis of **8**. The required 4-bromo-2-(2,2,2-trifluoro-1,1-dimethyl-ethyl)-pyridine **17** was prepared in two steps from the γ-pyrone **15** which in turn was prepared following an analogous procedure developed independently by Koreeda and Morgan.[30,31] After the direct arylation reaction, deprotection of the acetaminothiazole under acidic conditions was followed by the introduction of the prolineamide urea function in two steps via the imidazolide **20** to give the desired compound **8**. Treatment of 4-methyl-2-acetaminothiazole with appropriate 4-bromopyridine derivatives followed by prolineamide urea formation provided compounds **3**, **6**, and **9** (Table 1). Similarly, reaction of corresponding imidazolides with proline *N*-methylcarboxamide or pyrrolidine gave rise to the products **4** and **5**, respectively. Compounds **21** and **22** were prepared by using the reaction sequence shown in Scheme 1 but coupling 4-bromopyridine derivative **17** with 2-acetaminothiazole or 4-chloro-2-acetaminothiazole, respectively.

In the 5-(4-pyrimidinyl)-substituted aminothiazole series the key step was the build-up of the pyrimidine ring by reacting an appropriate amidine or guanidine derivative with the dimethylamino-vinyl ketone **24**. This is exemplified in Scheme 2 for the synthesis of compound **10**. As in the pyridine series, the prolineamide urea function was introduced in two steps to produce compounds **2**, **11**, **12**, **27** and **28**. The azetidine analog **7** was prepared by reacting the corresponding imidazolide with azetidine 2-carboxamide.

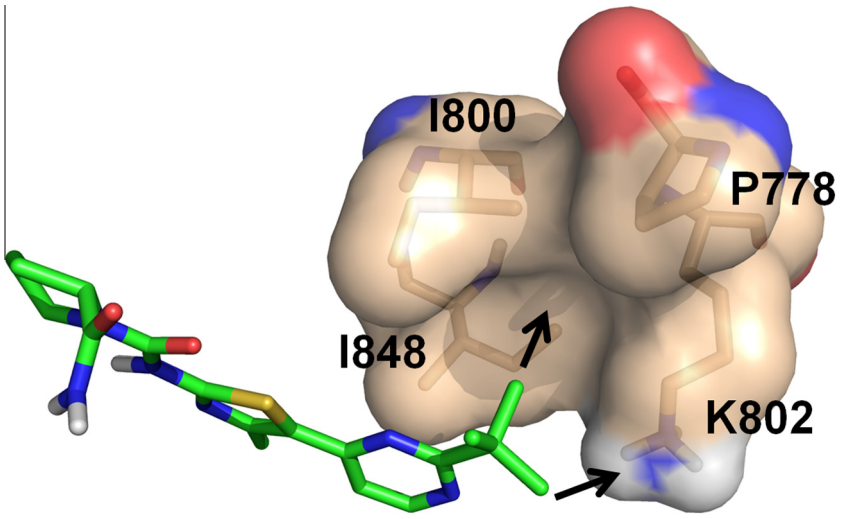

Figure 3. Detailed view of the binding model of **2** showing a small cavity formed by residues P778, I800, K802, and I848 proximal to the *tert*-butyl group of the compound.

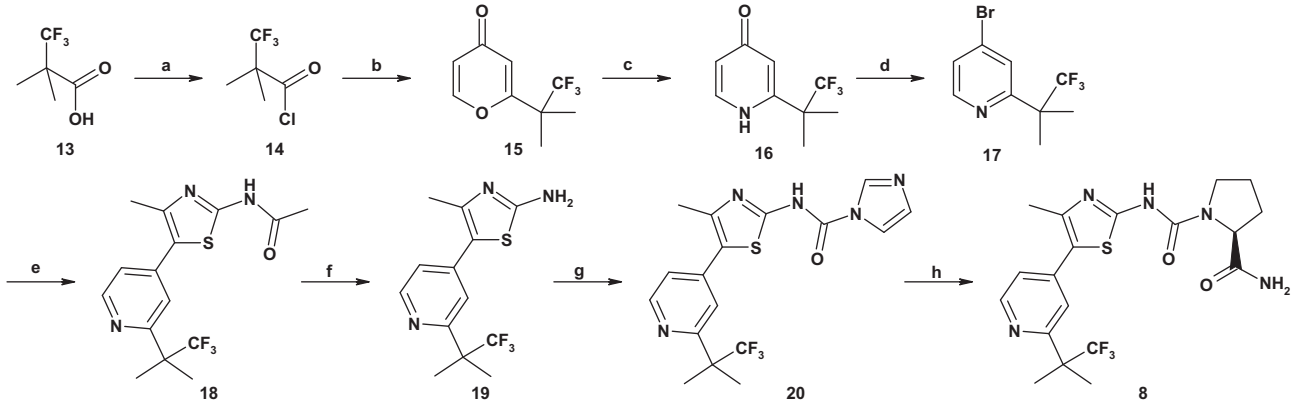

Scheme 1. Reagents and conditions: (a) Oxalyl chloride, chloroform, reflux, 4 h, quant; (b) (i) (*E*)-4-methoxy-3-buten-2-one and LiHMDS, THF, −78 °C, 1 h, then solution of the acid chloride in THF was added at −78 °C then in 2.5 h to rt, (ii) TFA, toluene, −10 °C to rt, 55%; (c) aqueous ammonia, 65 °C, 1 h, 65%. (d) $POBr_3$, 1,2-DCE, 85 °C, 1 h, 51%; (e) 4-methyl-2-acetamidothiazole, $Pd(OAc)_2$/$^tBu_3P{\cdot}HBF_4$, Cs_2CO_3, DMF, 120 °C, 2 h, 88%; (f) 6 N HCl, EtOH, 85 °C, 1 h, 95%; (g) CDI, DCM, reflux, 15 h, 83%; (h) L-prolineamide, Et_3N, DMF, rt, 15 h, 87%.

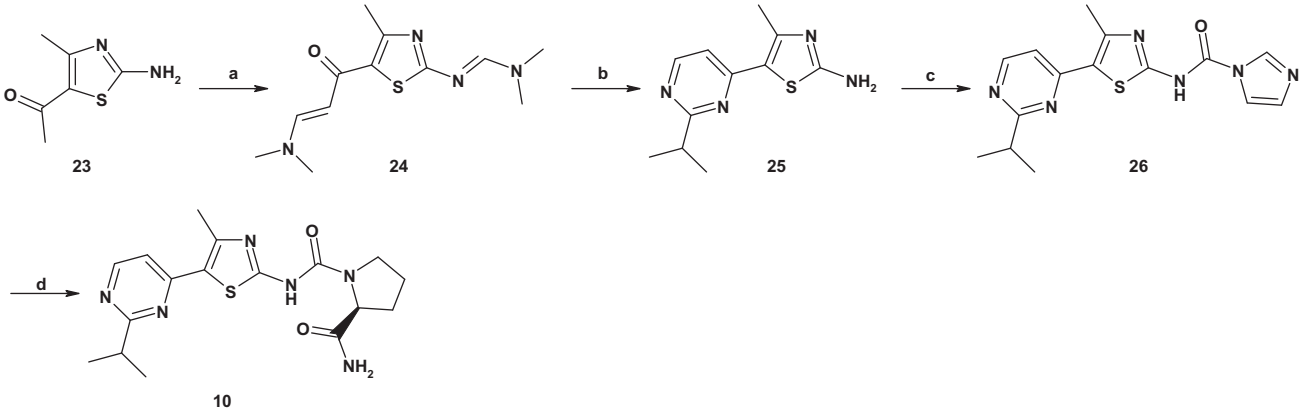

Scheme 2. Reagents and conditions: (a) DMF–DMA, reflux, 15 h, 32%; (b) *iso*-butyramidine hydrochloride, NaOH, 2-methoxyethanol, 125 °C, 1 h, 50%; (c) CDI, DMF, 80 °C, 15 h, 39%; (d) L-prolineamide, Et_3N, DMF, 40 °C, 15 h, 84%.

Encouraged by the biochemical results, the compounds were also tested in cellular assays measuring their ability to block the PI3K/Akt signaling pathway (Table 2).[32] The same trends in potency and selectivity as in the biochemical assays were observed. In particular, compounds **2**, **3** and **8** were able to produce a potent double digit nanomolar inhibition of PI3Kα-dependent Akt activation.

An assessment of the metabolic stability of compounds **2** and **3** was performed by incubation of these compounds with rat liver microsomes. This revealed two main metabolic pathways: hydrolysis of the primary amide to the carboxylic acid and aliphatic hydroxylation of either the *tert*-butyl group or the methyl substituent in 4-position of the thiazole ring (Fig. 4). With the aim to gain potency as previously mentioned but also to block one of the identified metabolic pathways, one of the methyls of the *tert*-butyl group was replaced by a trifluoromethyl substituent as exemplified by compounds **8** and **21**. This led to a significantly reduced in vitro clearance compared to compound **3** (Table 1). When in addition the 4-methyl group of the amino-thiazole in **8** was replaced by a chlorine atom, the clearance dropped even further (compound **22**). These findings indicate that both groups, the *tert*-butyl and the 4-methyl group, are major sites of metabolism in vitro for **3**. Replacement of the *tert*-butyl group by a 1-methyl-cyclopropyl one (compound **28** vs compound **2**) also gave a protective effect, although slightly lower than the trifluoromethyl substitution.

Table 2
Inhibition of Akt phosphorylation in Rat1-myr-p110x cells

Compound	IC_{50} (μM)		
	Rat1-myr-p110α	Rat1-myr-p110β	Rat1-myr-p110δ
1	0.13	2.1	0.62
2	0.039	3.1	1.5
3	0.061	8.0	0.72
4	>10	>10	5.8
5	2.5	>10	0.77
6	n.d	n.d.	n.d.
7	0.23	6.4	1.6
8	0.074	2.2	1.2
9	0.64	>10	>10
10	0.10	5.9	1.3
11	0.44	7.3	>10
12	4.6	>10	>10
21	0.14	2.4	2.9
22	0.34	>10	4.9
27	0.17	4.4	2.5
28	0.15	9.6	3.0

However, when incubated with rat liver microsomes, compound **28** led to the formation of reactive intermediates that could be trapped by glutathione.

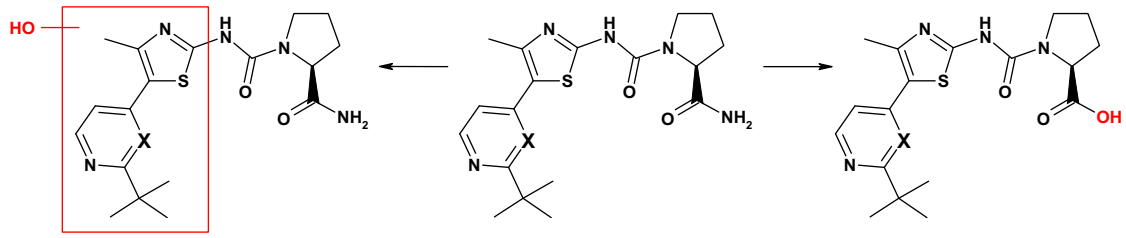

Figure 4. Main metabolic pathways of compounds **2** and **3** (X = N and X = CH, respectively) using rat liver microsomes.

Table 3
Pharmacokinetic parameters in female Sprague Dawley rats at 1 mg/kg iv, solution formulation NMP/PEG200 (30:70)

Compound		$t½$ (h)	CL in vivo/in vitro (mL min^{-1} kg^{-1})	V_{ss} (L/kg)	PPB[b] (%)
2	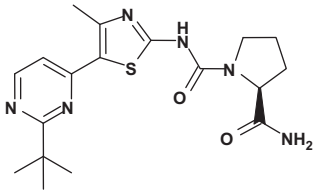	1.2 ± 0.1	21 ± 2/62[a]	1.2 ± 0.1	94.0
28	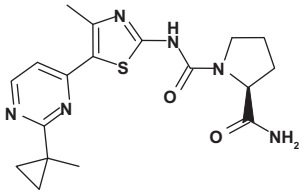	1.7 ± 0.0	8 ± 1/47	0.9 ± 0.1	97.1
3	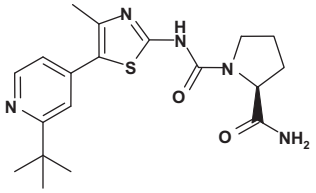	3.4 ± 1.6	39 ± 9/77[a]	1.4 ± 0.2	n.d.
8	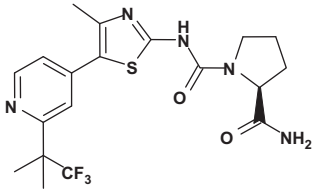	2.9 ± 0.2	10 ± 1/29	1.9 ± 0.1	94.3

[a] Includes the cofactor for glucuronyl transferases UDPGA.
[b] Plasma protein binding (%) in rat plasma.

In a next step, the pharmacokinetic parameters of selected compounds were assessed in rats (Table 3). As shown by the data in Tables 1 and 3 there was a reasonable correlation between in vitro and in vivo clearance. For both sets of compounds (**2** vs **28** and **3** vs **8**) the modification of the *tert*-butyl group led to a significantly reduced in vivo clearance. The half-life and volume of distribution of the compounds with the lower clearance **8** and **28** were moderate. In addition, compound **8** displayed excellent oral bioavailability in rats, mice and dogs (Table 4) and did not show any significant inhibition of the CYP450 enzymes. Moreover, it had no activity against the class III lipid kinase family member Vps34 and the related class IV PIKK protein kinases mTOR, DNA-PK and ATR in biochemical assays (IC_{50} >9.1 μM) and did not interfere with PIKKs involved in DNA-damage processes in cell-based assays (IC_{50} >10 μM on S15P-p53 and S1981P-ATM). The selectivity of compound **8** was also assessed against 442 kinases in different kinase panels (in-house, Invitrogen, Ambit). Overall, there was a higher than 50-fold selectivity window for p110α against all kinases tested and most of them were not inhibited at all at concentrations up to 10 μM.[33]

Table 4
Bioavailability of **8** (NVP-BYL719) in mice, rats, and dogs

Species	Doses	BAV (%)	CL in vivo (mL min^{-1} kg^{-1})	C_{max} p.o. dose normal (μM)
Mouse	1 mg/kg iv[a] 3 mg/kg p.o.[b]	106	8	0.52
Rat	3.4 mg/kg iv[c] 15 mg/kg p.o.[d]	58	10	0.19
Dog	0.1 mg/kg iv[a] 0.6 mg/kg p.o.[b]	140	8	1.07

[a] Solution in NMP:PEG200 (30:70).
[b] Solution in NMP:PEG300:SolutolHS15:water (10:30:20:40).
[c] Solution in PEG200/phosphate buffer pH 7.4 (2/1, v/v).
[d] Suspension in methylcellulose.

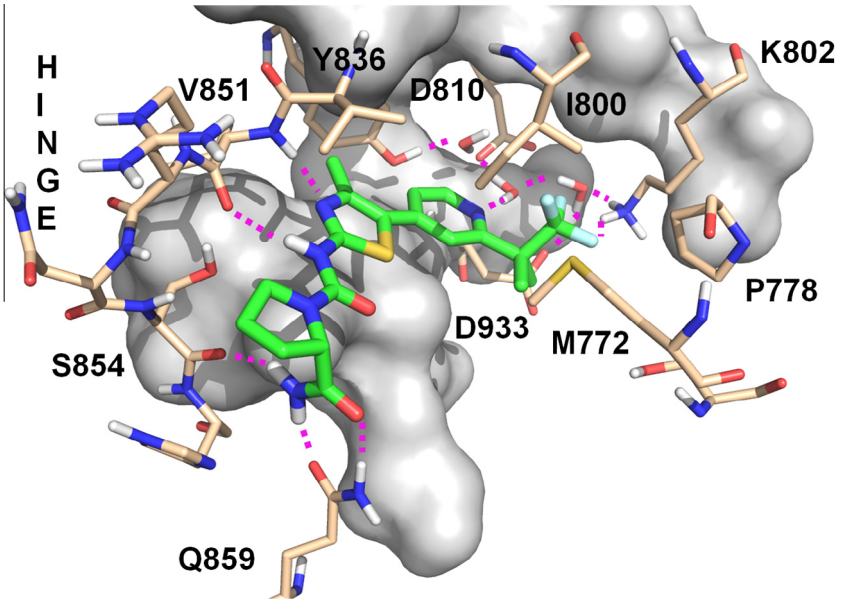

Figure 5. Crystal structure of PI3Kα in complex with **8**. Interactions of the compound with the ATP binding pocket. Hydrogen bonds are represented as dashed lines.

Based on its overall favorable profile compound **8** was selected for in vivo antitumor efficacy studies in nude mice where it showed dose-dependent inhibition of tumor growth. Its anti-tumor response in PIK3CA-dependent tumor models ranged from tumor stasis to tumor regression and the treatments were well tolerated by the animals.[33]

The binding model could be validated by the determination of the crystal structure of PI3Kα in complex with compound **8** at 2.2 Å resolution.[34] The co-crystal structure confirmed the existence of all the interactions inferred from docking **2** in the ATP pocket of the apo structure of PI3Kα. In particular, the pair of donor–acceptor hydrogen bonds between the inhibitor amide group and the side chain of Q859 was observed, fully backing the proposed structural PI3Kα selectivity concept. In addition, the X-ray structure revealed that the pyridine nitrogen atom of **8** is part of a hydrogen bond network involving three water molecules and the side chains of residues Y836, D810, D933 and K802, the latter residue also making a hydrogen bond with one of the fluorine atoms of the trifluoromethyl group. This is illustrated in Figure 5.

In summary, with compound **8** (NVP-BYL719) we have discovered a potent and selective PI3Kα inhibitor having a suitable ADME profile for pharmacological evaluation. The compound has shown good efficacy in inhibiting the growth of PI3Kα driven tumors in animal xenograft models as well as good tolerability.[33] It is now in clinical evaluation to assess its therapeutic potential for treating cancers in which the PIK3CA gene is mutated or amplified.

Acknowledgments

The authors would like to thank Mickael Le Douget, Vincent Bordas, Aurore Roustan, Dorothee Arz, Van Huy Luu, Jasmin Wirth, Susanne Vollmer, Philippe Ramstein and Werner Gertsch for their excellent technical assistance.

References and notes

1. Cantley, L. C. *Science* **2002**, *296*, 1655.
2. Katso, R.; Okkenhaug, K.; Ahmadi, K.; White, S.; Timms, J.; Waterfield, M. D. *Annu. Rev. Cell Dev. Biol.* **2001**, *17*, 615.
3. Samuels, Y.; Ericson, K. *Curr. Opin. Oncol.* **2006**, *18*, 77.
4. Hennessy, B. T.; Smith, D. L.; Ram, P. T.; Lu, Y.; Mills, G. B. *Nat. Rev. Drug Disc.* **2005**, *4*, 988.
5. Sansal, I.; Sellers, W. R. *J. Clin. Oncol.* **2004**, *22*, 2954.
6. Cheng, J. Q.; Godwin, A. K.; Bellacosa, A.; Taguchi, T.; Franke, T. F.; Hamilton, T. C.; Tsichlis, P. N.; Testa, J. R. *Proc. Natl. Acad. Sci. U.S.A.* **1992**, *89*, 9267.
7. Cheng, J. Q.; Ruggeri, B.; Klein, W. M.; Sonoda, G.; Altomare, D. A.; Watson, D. K.; Testa, J. R. *Proc. Natl. Acad. Sci. U.S.A.* **1996**, *93*, 3636.
8. Shayesteh, L.; Lu, Y.; Kuo, W. L.; Baldocchi, R.; Godfrey, T.; Collins, C.; Pinkel, D.; Powell, B.; Mills, G. B.; Gray, J. W. *Nat. Genet.* **1999**, *21*, 99.
9. Samuels, Y.; Velculescu, V. E. *Cell Cycle* **2004**, *3*, 1221.
10. Hartmann, C.; Bartels, G.; Gehlaar, C.; Hotkamp, N.; von Deimling, A. *Acta Neuropathol.* **2005**, *109*, 639.
11. Li, V. S.; Wong, C. W.; Chan, T. L.; Chan, A. S.; Zhao, W.; Chu, K. M.; So, S.; Chen, X.; Yuen, S. T.; Leung, S. Y. *BMC Cancer* **2005**, *5*, 29.
12. Lee, J. W.; Soung, Y. H.; Kim, S. Y.; Lee, H. W.; Park, W. S.; Nam, S. W.; Kim, S. H.; Lee, J. Y.; Yoo, N. J.; Lee, S. H. *Oncogene* **2005**, *24*, 1477.
13. Bachman, K. E.; Argani, P.; Samuels, Y.; Silliman, N.; Ptak, J.; Szabo, S.; Konishi, H.; Karabas, B.; Blair, B. G.; Lin, C.; Peters, B. A.; Velculescu, V. E.; Park, B. H. *Cancer Biol. Ther.* **2004**, *3*, 772.
14. Campbell, I. G.; Russell, S. E.; Choong, D. Y.; Motgomery, K. G.; Ciavarella, M. L.; Hooi, C. S.; Cristiano, B. E.; Pearson, R. B.; Phillips, W. A. *Cancer Res.* **2004**, *64*, 7678.
15. Levine, D. A.; Bogomolniy, F.; Yee, C. J.; Lash, A.; Barakat, R. R.; Borgen, P. I.; Boyd, J. *Clin. Cancer Res.* **2005**, *11*, 2875.
16. Wu, G.; Xing, M.; Mambo, E.; Huang, X.; Liu, X.; Guo, Z.; Chatterjee, A.; Goldenberg, D.; Gollin, S. M.; Sukumar, S.; Trink, B.; Sidransky, D. *Breast Cancer Res.* **2005**, *7*, R609.
17. Folkes, A. J.; Ahmadi, K.; Alderton, W. K.; Alix, S.; Baker, S. J.; Box, G.; Chuckowree, I. S., et al *J. Med. Chem.* **2008**, *51*, 5522.
18. Emerling, B. M.; Akcakanat, A. *Cancer Res.* **2011**, *71*, 7351.
19. Burger, M. T.; Pecchi, S.; Wagman, A.; Ni, Z.-J.; Knapp, M.; Hendrickson, T.; Atallah, G.; Pfister, K.; Zhang, Y.; Bartulis, S.; Frazier, K.; Ng, S.; Smith, A.; Verhagen, J.; Haznedar, J.; Huh, K.; Iwanowicz, E.; Xin, X.; Menezes, D.; Merritt, H.; Lee, I.; Wiesmann, M.; Kaufman, S.; Crawford, K.; Chin, M.; Bussiere, D.; Shoemaker, K.; Zaror, I.; Maira, S.-M.; Voliva, C. F. *ACS Med. Chem. Lett.* **2011**, *2*, 774.
20. Yaguchi, S.; Fukui, Y.; Koshimizu, I.; Yoshimi, H.; Matsuno, T.; Gouda, H.; Hirono, S.; Yamazaki, K.; Yamori, T. *J. Natl. Cancer Inst.* **2006**, *98*, 545.
21. Ohwada, J.; Ebiike, H.; Kawada, H.; Tsukazaki, M.; Nakamura, M.; Miyazaki, T.; Morikami, K.; Yoshinari, K.; Yoshida, M.; Kondoh, O.; Kuramoto, S.; Ogawa, K.; Aoki, Y.; Shimma, N. *Bioorg. Med. Chem. Lett.* **2011**, *21*, 1767.
22. Bruce, I.; Akhlaq, M.; Bloomfield, G. C.; Budd, E.; Cox, B.; Cuenoud, B.; Finan, P.; Gedeck, P.; Hatto, J.; Hayler, J. F.; Head, D.; Keller, T.; Kirman, L.; Leblanc, C.; Le Grand, D.; McCarthy, C.; O'Connor, D.; Owen, C.; Oza, M. S.; Pilgrim, G.; Press, N. E.; Sviridenko, L.; Whitehead, L. *Bioorg. Med. Chem. Lett.* **2012**, *22*, 5445.
23. Huang, C.-H.; Mandelker, D.; Schmidt-Kittler, O.; Samuels, Y.; Velculescu, V. E.; Kinzler, K. W.; Vogelstein, B.; Gabelli, S. B.; Amzel, L. M. *Science* **2007**, *318*, 1744. PDB code 2RD0.
24. Using a version of MacroModel enhanced for graphics by A. Dietrich, the compound was manually constructed and docked in the ATP pocket and the resulting ligand–protein complex energy-minimized using the AMBER*/H_2O/GBSA force field. MacroModel: Mohamadi, F.; Richards, N. G. J.; Guida, W. C.; Liskamp, R.; Lipton, M.; Caufield, C.; Chang, G.; Hendrickson, T.; Still, W. C. *J. Comput. Chem.* **1990**, *11*, 440.

25. Knight, Z. A.; Gonzalez, B.; Feldman, M. E.; Zunder, E. R.; Goldenberg, D. D.; Williams, O.; Loewith, R.; Stokoe, D.; Balla, A.; Toth, B.; Balla, T.; Weiss, W. A.; Williams, R. L.; Shokat, K. M. *Cell* **2006**, *125*, 733.
26. The biochemical inhibitory activities of the compounds were measured using Kinase-Glo® assays for the α and β isoforms. Adapta® assays were used for the δ and γ isoforms. For a detailed description of the Kinase-Glo® assays used see: Caravatti, G., Fairhurst, R. A.; Furet, P.; Guagnano, V.; Imbach, P. PCT Int. Pat. Appl. WO 2010/029082, March 18, 2010. The Adapta® assays were run as follows: 50 nL of compound dilutions were dispensed onto white 384-well small volume polystyreneplate. Then 5 μL of PI3K and lipid substrate (PI or PIP2:PS) followed by 5 μL of ATP (final assay volume 10 μL) are incubated at RT. The standard reaction buffer for the Adapta® TR-FRET assay contained 10 mM Tris–HCl pH 7.5, 3 mM $MgCl_2$, 50 mM NaCl, 1 mM DTT, 0.05% CHAPS (v/v). Reactions were stopped with 5 μL of a mixture of EDTA containing the Eu^{3+}-labeled anti-ADP antibody and the Alexa Fluor® 647-labeled ADP tracer in TR-FRET dilution buffer (proprietary to IVG). Plates were read 15–60 min later in a Synergy2 reader using an integration time of 0.4 s and a delay of 0.05 s. Control for the 100% inhibition of the kinase reaction was performed by replacing the PI3K by the standard reaction buffer. The control for the 0% inhibition was given by the solvent vehicle of the compounds (90% DMSO in H_2O, v/v). A reference compound was included in all assay plates in the form of 16 dilution points in duplicate.
27. The accuracy of our bioassays is exemplified by compound **28** (IC_{50} ± SEM (*n*)): p110α 0.012 ± 0.001 (16); p110β 3.1 ± 0.30 (15); p110δ 0.81 ± 0.16 (5); p110γ 0.69 ± 0.21 (5); Rat1α 0.15 ± 0.027 (5); Rat1β >10 (4); Rat1δ 3.0 ± 0.65 (5).
28. A *tert*-butyl group has a volume of around 80 $Å^3$ against 90 $Å^3$ for the diethylamino group. The dimethylamino group is significantly smaller with a volume of around 60 $Å^3$.
29. Yokooji, A.; Okazawa, T.; Satoh, T.; Miura, M.; Nomura, M. *Tetrahedron* **2003**, *59*, 5685.
30. Koreeda, M.; Akagi, H. *Tetrahedron Lett.* **1980**, *21*, 1197.
31. Morgan, T. A.; Ganem, B. *Tetrahedron Lett.* **1980**, *21*, 2773.
32. The compounds were tested for their ability to inhibit the phosphorylation of Akt serine 473 in Rat1 cell lines overexpressing activated versions of each class IA PI3K isoform. For a description of these assays see: Maira, S. M. et al *Mol. Cancer Ther.* **2012**, *11*, 317.
33. Fritsch, C. et al. in preparation.
34. The details of this X-ray structure determination will be published elsewhere: Knapp, M. et al. in preparation. The coordinates have been deposited with PDB ID code 4JPS.